Composites Part B 132 (2018) 151–160

Contents lists available at ScienceDirect

Composites Part B

journal homepage: www.elsevier.com/locate/compositesb

Determination of the excitation frequencies of laminated orthotropic non-homogeneous conical shells

A.H. Sofiyev [a, *], N. Kuruoglu [b]

[a] Department of Civil Engineering of Engineering Faculty, Suleyman Demirel University, Isparta, Turkey
[b] Department of Civil Engineering of Faculty of Engineering and Architecture, Istanbul Gelisim University, Istanbul, Turkey

ARTICLE INFO

Article history:
Received 2 May 2017
Received in revised form
22 June 2017
Accepted 28 August 2017
Available online 6 September 2017

Keywords:
Layered structures
Vibration
Analytical modelling
Numerical analysis

ABSTRACT

The excitation frequencies of parametric vibration of laminated non-homogeneous orthotropic conical shells (LNHOCSs) under axial load periodically varying with time, are determined using the classical shell theory (CST). The basic equations are found using the Donnell-Mushtari shell theory and reduce to the Mathieu-Hill type differential equation, in which the instability is examined by the Bolotin method. To validate of current results was made a comparison with the previous studies. The effects of stacking sequences, axial load factors, non-homogeneity, as well as the variation of geometric characteristics on the backward and forward excitation frequencies (BFEFs) of conical shells are studied in detail.

1. Introduction

Layered conical shells are widely used in the aerospace and marine industries due to advantages such as high rigidity to weight and durability, as well as low operating costs. Layered shells can be subjected to dynamic loads under various operating conditions. Thus, the vibration behavior of layered conical shells under dynamic loading is critical for safety and reliability. Among the dynamic problems have been widely studied the free vibrations of homogeneous multilayer conical shells and there are many studies in the literature [1–24].

Modern laminates are inhomogeneous with heterogeneities ranging from a nanoscale to a macroscale [25]. One of the areas of interest is the study of the behavior of the mechanical properties of inhomogeneous layered shells under dynamic periodic loading. Compared to laminated homogeneous shells, the adoption of continuous change of material properties of the layers can provide important benefits. Indeed, the increase in the number of constructive variables extends the possibilities of advanced composite materials, as well as stability and vibration behaviors may be significantly improved. The first basic knowledge on the changes of the material properties is given in the works of Lomakin [26] and Khoroshun et al. [27]. Following these works, numerous studies in this subject have been published in the literature [28–39].

The studies on the parametric vibration of laminated shells are relatively scarce and most of these works are devoted laminated cylindrical shells. One of first study on the solution of the parametric vibration of laminated anisotropic shells is proposed by Goroshko and Emelyanenko [40]. The instability zones of laminated orthotropic cylindrical shell under periodic loads are presented by Argento and Scott [41,42]. The dynamic instability of layered shells under different form of time dependent loads have analyzed by Liao and Cheng [43,44], Lam and Loy [45], and Ng and Lam [46]. A comprehensive bibliography of papers on the parametric vibration of structural elements from 1987 to 2005, are presented by Sahu and Datta [47]. The dynamic instability of layered composite plates and cylindrical shells subjected to uniform and non-uniform axial loads has been studied by Fazilati and Ovesy [48,49]. The dynamic and parametric instability of composite panels is investigated by Dey and Ramachandra [50] and Panda et al. [51], respectively. Dynamic instability analysis for S-FGM plates embedded in Pasternak elastic medium using the modified couple stress theory is studied by Park et al. [52]. Lei et al. [53] presented parametric analysis of frequency of rotating laminated CNT reinforced FG cylindrical panels. Sahmani and Aghdam [54] studied instability of hydrostatic pressurized hybrid FGM exponential shear deformable nanoshells based on the nonlocal continuum elasticity. Li et al. [55]

* Corresponding author. Department of Civil Engineering of Engineering Faculty, Suleyman Demirel University, 32260 Isparta, Turkey.
E-mail address: abdullahavey@sdu.edu.tr (A.H. Sofiyev).

http://dx.doi.org/10.1016/j.compositesb.2017.08.013
1359-8368/

investigated nonlocal vibration and stability in parametric resonance of axially moving nanoplate. Akhavan and Ribeiro [56] presented geometrically non-linear periodic forced vibrations of imperfect laminates with curved fibers by the shooting method.

The foregoing brief literature survey reveals that excitation frequencies of parametric vibration of LNHOCS under axial load periodically varying with time have not been investigated to date. This task is undertaken in the current study.

2. Basic relations

The LNHOCS which composed of N layers of equal thickness, as shown in Fig. 1. Terms of contact between any two adjacent layers is absolutely rigid connection that satisfies Kirchhoff-Love hypothesis for the entire shell. The coordinate system $(Or\theta z)$ is located on the mid-surface, in which r, z and θ are axes in the meridional direction, normal to the r axis and in the direction perpendicular to the (Sz) surface, respectively. The orthotropy axes are parallel to the r and θ.

The elasticity moduli of non-homogeneous material of the layer (k+1) are defined as:

$$\begin{bmatrix} E_r^{(k+1)}(z_1), E_\theta^{(k+1)}(z_1), G^{(k+1)}(z_1),\ \rho^{(k+1)}(z_1) \end{bmatrix} = \eta_1^{(k+1)}(z_1)\left[E_{0r}^{(k+1)}, E_{0\theta}^{(k+1)}, G_0^{(k+1)}, \rho_0^{(k+1)}\right], z_1 = z/h \tag{1}$$

where $-h/2 + kh/N \le z \le -h/2 + (k+1)h/N, \quad k = 0, 1, \ldots, (N-1)$, $E_{0r}^{(k+1)}$, $E_{0\theta}^{(k+1)}$ and $G_0^{(k+1)}$ are elasticity moduli of homogeneous (H) materials in the layer, $(k+1)$. Additionally, $\eta_1^{(k+1)}(z_1) = 1 + \mu\eta^{(k+1)}(z_1)$, where $\eta^{(k+1)}(z_1)$ denote the variations of the elasticity moduli in the layers and are continuous functions and μ is a variation coefficient of material properties and satisfied the condition $0 \le \mu \le 1$ [30]. The density of H orthotropic materials, $\rho_0^{(k+1)}$, and Poisson's ratios in the layer $(k+1)$, $\nu_{r\theta}^{(k+1)}$ and $\nu_{\theta r}^{(k+1)}$, are assumed to be constant and $\nu_{\theta r}^{(k+1)} E_{0r}^{(k+1)} = \nu_{r\theta}^{(k+1)} E_{0\theta}^{(k+1)}$ [57,58].

Assume that the LNHOCS under the axial load periodically varying with time,

$$n_r^0 = -P(t) = -P_s - P_d\cos(\Lambda t),\quad n_\theta^0 = 0,\quad n_{r\theta}^0 = 0 \tag{2}$$

where n_r^0, n_θ^0 and $n_{r\theta}^0$ are the membrane forces, P_s and P_d are the static axial load and the amplitude of the time dependent periodic axial load, and Λ is the excitation frequency and t is a time variable [59].

The relationships between stresses and strains for a non-homogeneous orthotropic lamina (k+1), in thin conical shells within the Donell-Mushtari theory can be expressed as

$$\begin{bmatrix} \tau_r^{(k+1)} \\ \tau_\theta^{(k+1)} \\ \tau_{r\theta}^{(k+1)} \end{bmatrix} = \begin{bmatrix} E_{11}^{(k+1)} & E_{12}^{(k+1)} & 0 \\ E_{12}^{(k+1)} & E_{22}^{(k+1)} & 0 \\ 0 & 0 & E_{66}^{(k+1)} \end{bmatrix} \times \begin{bmatrix} \varepsilon_r^0 - z\dfrac{\partial^2 w}{\partial r^2} \\ \varepsilon_\theta^0 - z\left(\dfrac{1}{r^2}\dfrac{\partial^2 w}{\partial\theta_1^2} + \dfrac{1}{S}\dfrac{\partial w}{\partial r}\right) \\ \varepsilon_{r\theta}^0 - z\left(\dfrac{1}{r}\dfrac{\partial^2 w}{\partial r\,\partial\theta_1} - \dfrac{1}{r^2}\dfrac{\partial w}{\partial\theta_1}\right) \end{bmatrix} \tag{3}$$

where $\tau_r^{(k+1)}, \tau_\theta^{(k+1)}, \tau_{r\theta}^{(k+1)}$ are the stresses in the layer, $(k+1)$, $\varepsilon_r^0, \varepsilon_\theta^0, \varepsilon_{r\theta}^0$ are the deformations on the reference surface and the quantities $E_{ij}^{(k+1)}$, $(i,j = 1,2,6)$, are defined as

$$E_{11}^{(k+1)} = \frac{E_{0r}^{(k+1)}\eta_1^{(k+1)}(z_1)}{1 - \nu_{r\theta}^{(k+1)}\nu_{\theta r}^{(k+1)}},\quad E_{12}^{(k+1)} = \nu_{\theta r}^{(k+1)}E_{11}^{(k+1)} = \nu_{r\theta}^{(k+1)}E_{22}^{(k+1)},$$
$$E_{22}^{(k+1)} = \frac{E_{0\theta}^{(k+1)}\eta_1^{(k+1)}(z_1)}{1 - \nu_{r\theta}^{(k+1)}\nu_{\theta r}^{(k+1)}},\quad E_{66}^{(k+1)} = 2G_0^{(k+1)}\eta_1^{(k+1)}(z_1). \tag{4}$$

The force and moment resultants of LNHOCSs are expressed by the following relations:

$$[(n_r, n_\theta, n_{r\theta}), (m_r, m_\theta, m_{r\theta})] = \sum_{k=0}^{N-1}\int_{-0.5h+kh/N}^{-0.5h+(k+1)h/N} \times \left[\tau_r^{(k+1)}, \tau_\theta^{(k+1)}, \tau_{r\theta}^{(k+1)}\right][1, z]\mathrm{d}z \tag{5}$$

The Airy stress function, $\Psi(r,\theta,t)$, is introduced by the following relations [58]:

$$(n_r, n_\theta, n_{r\theta}) = \frac{1}{r^2}\left(\frac{\partial^2\Psi}{\partial\theta_1^2} + r\frac{\partial\Psi}{\partial r},\ r^2\frac{\partial^2\Psi}{\partial r^2},\ -r\frac{\partial^2\Psi}{\partial r\partial\theta_1} + \frac{\partial\Psi}{\partial\theta_1}\right) \tag{6}$$

3. Basic equations

The basic equations of LNHOCSs taking into account Eqs. (1) and (2) are expressed as [30,58]:

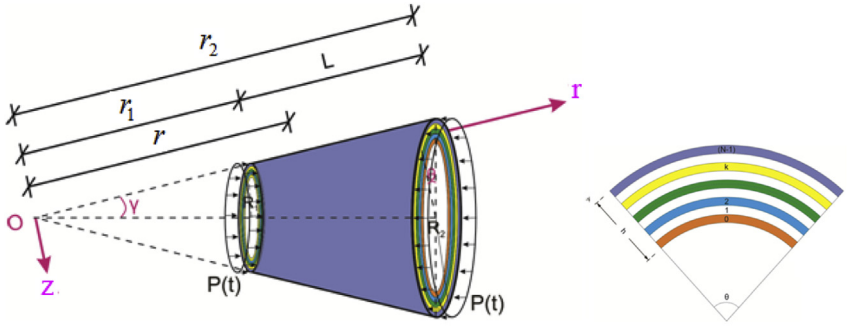

a) b)

Fig. 1. **(a)** The LNHOCS under axial load periodically varying with time and **(b)** laminate schema.

$$\frac{\partial^2 m_r}{\partial r^2}+\frac{2}{r}\frac{\partial m_r}{\partial r}+\frac{2}{r}\frac{\partial^2 m_{r\theta}}{\partial r\partial\theta_1}-\frac{1}{r}\frac{\partial m_\theta}{\partial r}+\frac{2}{r^2}\frac{\partial m_{r\theta}}{\partial\theta_1}+\frac{1}{r^2}\frac{\partial^2 m_\theta}{\partial\theta_1^2}+\frac{n_\theta}{r}\cot\gamma +[P_s+P_d\cos(\Lambda t)]\frac{\partial^2 w}{\partial r^2}-\rho_1\frac{\partial^2 w}{\partial t^2}=0 \tag{7}$$

$$\frac{\cot\gamma}{r}\frac{\partial^2 w}{\partial r^2}-\frac{2}{r}\frac{\partial^2\varepsilon^0_{r\theta}}{\partial r\partial\theta_1}-\frac{2}{r^2}\frac{\partial\varepsilon^0_{r\theta}}{\partial\theta_1}+\frac{\partial^2\varepsilon^0_\theta}{\partial r^2}+\frac{1}{r^2}\frac{\partial^2\varepsilon^0_r}{\partial\theta_1^2}+\frac{2}{r}\frac{\partial\varepsilon^0_\theta}{\partial r}-\frac{1}{r}\frac{\partial\varepsilon^0_r}{\partial r}=0 \tag{8}$$

where

$$\rho_1=\sum_{k=0}^{N-1}\int_{-0.5h+kh/N}^{-0.5h+(k+1)h/N}\rho_0^{(k+1)}dz \tag{9}$$

Substitution of Eq. (3) into Eq. (5) yields the expressions for moments and strains of LNHOCSs, being substituted in Eqs. (7) and (8), together with relations (2) and (6), the dynamic stability and compatibility equations can be expressed as:

$$\begin{bmatrix}L_{11}L_{12}\\L_{21}L_{22}\end{bmatrix}\begin{bmatrix}\Psi_1\\w\end{bmatrix}=0 \tag{10}$$

where $\Psi=\Psi_1 e^{2x}$ is considering instead of Ψ, $x=\ln(r/r_1)$ is the new variable and $L_{ij}(i,j=1,2)$ are the differential operators and are given in Appendix A.

The system of Eq. (10) may be used for the parametric vibration of LNHOCSs.

4. Solution of basic equations

If the LNHOCS assumed under simply-supported boundary conditions, the solution is sought in he following form [58]:

$$w=f(t)e^x\sin(m_1x)\sin(m_2\theta) \tag{11}$$

where $f(t)$ is the function depending on the time and are given the following symbols:

$$m_1=\frac{m\pi}{x_0},\quad m_2=\frac{n}{\sin\gamma},\quad x_0=\ln\frac{r_2}{r_1} \tag{12}$$

in which m and n are wave numbers in the meridional and circumferential directions.

Substitution of Eq. (14) into Eq. (11) and using Superposition method one gets:

$$\Psi_1=f(t)\begin{bmatrix}U_1\sin(m_1x)\sin(m_2\theta_1)+U_2\cos(m_1x)\sin(m_2\theta_1)\\+U_3e^{-x}\sin(m_1x)\sin(m_2\theta_1)+U_4e^{-x}\cos(m_1x)\sin(m_2\theta_1)\end{bmatrix} \tag{13}$$

The following notation was introduced:

$$U_1=\frac{z_{11}x_{11}+y_{11}z_{12}}{x_{11}^2+y_{11}^2},U_2=\frac{x_{11}z_{12}-z_{11}y_{11}}{x_{11}^2+y_{11}^2},$$
$$U_3=\frac{m_1(m_1y_{01}-x_{01})r_1\cot\gamma}{x_{01}^2+y_{01}^2},\quad U_4=\frac{m_1(m_1x_{01}+y_{01})r_1\cot\gamma}{x_{01}^2+y_{01}^2} \tag{14}$$

in which

$$\begin{aligned}
x_{01}&=-q_3m_1^2+q_5m_1^2m_2^2-q_7m_2^2+q_1m_1^4+q_8m_2^4,\\
y_{01}&=q_2m_1^3-q_4m_1+q_6m_1m_2^2,\\
x_{11}&=q_5m_1^2m_2^2+(3q_2-6q_1-q_3)m_1^2\\
&+(q_6-q_7-q_5)m_2^2+q_1m_1^4+q_8m_2^4\\
&+q_1-q_2+q_3-q_4,\\
y_{11}&=(q_6-2q_5)m_1m_2^2+\\
&(2q_3-q_4+4q_1-3q_2)m_1+(q_2-4q_1)m_1^3,\\
z_{11}&=\vartheta_{14}\left[\left(m_2^2-1\right)^2+m_1^2\right]\\
&+m_1^2\left[(\vartheta_{24}+\vartheta_{13}-2\vartheta_{32})m_2^2+\left(m_1^2+1\right)\vartheta_{23}\right],\\
z_{12}&=m_1\left(m_2^2-m_1^2-1\right)(\vartheta_{24}-\vartheta_{13}),\\
q_1&=\vartheta_{22},q_2=-4\vartheta_{22},q_3=5\vartheta_{22}-\vartheta_{11},\\
q_4&=-2\vartheta_{22}+2\vartheta_{11},q_5=2\vartheta_{31}+2\vartheta_{21},\\
q_6&=-4\vartheta_{31}-4\vartheta_{12},q_7=2(\vartheta_{31}+\vartheta_{21}+\vartheta_{11}),q_8=\vartheta_{11}.
\end{aligned} \tag{15}$$

Substituting Eqs. (11) and (13) into second equation of the set (10), then employing the Galerkin's method to the resulting equation in the parts $0\le\theta_1\le 2\pi\sin\gamma$ and $0\le x\le x_0$, and after integrations, one gets,

$$\frac{d^2f(t)}{dt^2}+\frac{K-u_{ax}[P_s+P_d\cos(\Lambda t)]}{u_\rho\rho_1}f(t)=0 \tag{16}$$

where K, u_{ax} and u_ρ are the coefficients that define the properties of the LNHOCSs and are presented in Appendix B in detail.

Eliminating static and periodic axial loads from Eq. (16), we can obtain expressions for dimensional frequency and dimensionless frequency parameters (DFP) of LNHOCSs:

$$\omega=\sqrt{\frac{(U_3-2m_1U_1/3)u_1+(U_2-\beta_1U_4)u_2+u_3}{u_\rho\rho_1}} \tag{17}$$

and

$$\omega_1=\omega R_1\sqrt{\left[1-\left(\nu_{r\theta}^{(k+1)}\right)^2\right]\rho_0^{(k+1)}\Big/E_{0r}^{(k+1)}} \tag{18}$$

To solve the instability problem, Eq. (16) is transformed into the following Mathieu–Hill type differential equation [59]:

$$\frac{d^2f(t)}{dt^2}+\omega^2[1-P_{s1}-P_{d1}\cos(\Lambda t)]f(t)=0 \tag{19}$$

where $P_{s1}=P_s/P_{crst}^{ax}$ and $P_{d1}=P_d/P_{crst}^{ax}$ denote the static and dynamic axial load factors, and P_{crst}^{ax} denotes the critical static axial load.

It is well-known that the periodic solutions of Eq. (19) with period $2T(T=2\pi/\Lambda)$ are of practical importance, thus the periodic solution may be written as [59].

$$f(t)=\sum_{i=1,3,5,\ldots}^{\infty}\overline{a}_i\cos\left(\frac{\Lambda t}{2}\right)+\overline{b}_i\sin\left(\frac{\Lambda t}{2}\right) \tag{20}$$

where $\overline{a}_i$ and $\overline{b}_i$ are arbitrary coefficients need to be found.

Introducing of (20) into Eq. (19) and if we consider first term of the series, then by grouping the sine and cosine terms and eliminating terms with the triple frequency, the equation can be simplified as

$$\left[-\Lambda^2+4\omega^2(1-P_{s1}-0.5P_{d1})\right]\overline{a}_1\cos\left(\frac{\Lambda t}{2}\right)+\left[-\Lambda^2+4\omega^2(1-P_{s1}+0.5P_{d1})\right]\overline{b}_1\sin\left(\frac{\Lambda t}{2}\right)=0 \tag{21}$$

As $\overline{a}_1\neq0$ and $\overline{b}_1\neq0$, from Eq. (21), we get the expressions for the dimensionless excitation frequency of LNHOCSs:

$$\Lambda_{11}=2\omega\sqrt{1-P_{s1}-0.5P_{d1}} \tag{22}$$

and

$$\Lambda_{12}=2\omega\sqrt{1-P_{s1}+0.5P_{d1}} \tag{23}$$

where Λ_{11} and Λ_{12} are denote backward and forward excitation frequencies (BFEFs) of LNHOCSs based on the CST for certain mode (m,n).

The dimensionless BFEFs, i.e., $\overline{\Lambda}_{1j}$, are defined as:

$$\overline{\Lambda}_{1j}=2\pi R_1\Lambda_{1j}\sqrt{\left[1-\left(\nu_{r\theta}^{(k+1)}\right)^2\right]\rho_0^{(k+1)}\Big/E_{0r}^{(k+1)}},\quad(j=1,2) \tag{24}$$

When $P_{d1}=0$, from Eqs. (22) and (23), the formula for the point of origin of main instability zones for LNHOCSs is obtained.

5. Results and discussion

5.1. Comparison with literature

The results of accomplished convergence and verification analyses are presented in this subsection. The first verification example is associated with the magnitudes of origin of main instability regions of laminated homogeneous orthotropic (LHO) cylindrical shells with lamination (9/0/9) are given in Table 1 and are compared with those of Ng and Lam [46] used Donnell, Love and Flugge theories. If $\mu=0$ and $\gamma\to0$ are considered in Eq. (24), the expression for LNHOCSs are converted into the expression for LHO cylindrical shells. The input parameters are taken from Ng and Lam [46]: $L_1/R=2$ and $R/h=200$, $E_{0r}^{(k+1)}/E_{0\theta}^{(k+1)}=40, G_0^{(k+1)}/E_{0\theta}^{(k+1)}=0.5$, $\nu_{r\theta}^{(k+1)}=0.25$ and $\rho_0^{(k+1)}=1$, $k=2$, $(m,n)=(1,4)$ and $P_{s1}=0.3$. It is seen that the present results are in good agreement with results of Ng and Lam [46], within the Donnell shell theory.

Table 1
Comparison of the values of origin of main instability zones for LHO cylindrical shells with the lamination (9/0/9).

	Ng and Lam [46]	Present study
Theories	$\Lambda_{11}=\Lambda_{12}$	$\Lambda_{11}=\Lambda_{12}$
Donnell	92.7717	92.8022
Love	91.2511	
Flugge	91.2498	

In the second verification example, the values of DFP, $\omega_1=\omega R_2\sqrt{[1-\nu_{r\theta}^{(k+1)}\nu_{\theta r}^{(k+1)}]\rho_0^{(k+1)}/E_{0r}^{(k+1)}}$, $(k=1$ and $9)$ for the laminated homogeneous orthotropic conical shells (LHOCSs) with laminations $(0/9)_2$ and $(0/9)_{10}$ are compared with the results of Shu [5], and Wu and Lee [29], and presented in Table 2. By taking $\mu=0$ into Eq. (18), the expression for the DFP of the LNHOCS is transformed to the expression for the LHOCS. The geometries of the truncated conical shell are given as $\gamma=\pi/6;\ L=0.5R_2;\ R_2=100h$. The material properties of the lamina are, $E_{0r}^{(k+1)}/E_{0\theta}^{(k+1)}=15;\ G_0^{(k+1)}/E_{0\theta}^{(k+1)}=0.5;$ $\nu_{r\theta}^{(k+1)}=0.25;\nu_{\theta r}^{(k+1)}=\nu_{r\theta}^{(k+1)}E_{0\theta}^{(k+1)}/E_{0r}^{(k+1)};\rho_0^{(k+1)}=1;k=1$ and 9, are given in Ref. [29]. Our numerical results show good agreement with those of Refs. [5] and [29].

In the third verification example, the values of the DFP $\omega_1=\omega(L_1^2/h)\sqrt{\rho^{(k+1)}/E_{0\theta}^{(k+1)}}$, $k=2$ and 3 for LHO cylindrical shells of lamination schemes (0/9/0) or (0/9/9/0) are compared with those of Ferreira et al. [14] and Ye and Soldatos [60], and given in Table 3. The LHOCS transformed to the LHO cylindrical shell, as $\gamma\to0^\circ, R_2\approx R_1\approx R$ and $L=L_1$ is taken into account in Eq. (18). Here R and L_1 are the radius and length of the LHO cylindrical shell, respectively, and the thickness of each layer is constant. The cylindrical shell characteristics and the material properties in the lamina are, $R/L_1=5;\ 10, L_1/h=100$ and $E_{0r}^{(k+1)}=25E_{0\theta}^{(k+1)},\quad G_0^{(k+1)}=E_{0\theta}^{(k+1)}/2,\quad \nu_{r\theta}^{(k+1)}=1/4,\ \rho_0^{(k+1)}=1,$ $k=2,3$ and were taken from Ref. [14]. The meridional wave number is taken to be $m=1$. The buckling parameters show good agreement with those of obtained from the solution given in Refs. [14] and [60] for various radius to length ratios.

5.2. Variation of dimensionless backward and forward excitation frequencies (BFEFs) of LNHOCSs

In this subsection, the novel results for LNHOCSs with several stacking sequences are proposed to study the variation of dimensionless backward and forward excitation frequencies using the expression (24). In numerical computations, $m=1$ and the excitation frequencies are minimized only versus the circumferential wave number, n. For each case, three different lamination schemes are contemplated. In particular, a single layer made of Glass-Epoxy oriented of (0), three and four plies made all of the same material arranged as (0/9/0) and (0/9/9/0), respectively, are considered. In each circumstance, h is 0.01 m. As explained before, the solution is obtained in the framework for the Kirchhoff-Love hypothesis.

The material of lamina is assumed to be Glass-Epoxy composites, with the following homogeneous orthotropic properties: $E_{0r}^{(k+1)}=53.7791\times10^{11}Pa,\quad E_{0\theta}^{(k+1)}=17.9264\times10^{9}Pa,\quad G_0^{(k+1)}=8.9632\times10^{9}Pa,\ \nu_{\theta r}^{(k+1)}=\nu_{r\theta}^{(k+1)}E_{0\theta}^{(k+1)}/E_{0r}^{(k+1)},\ \nu_{r\theta}^{(k+1)}=0.25$ and $\rho_0^{(k+1)}=1900\ kg/m^3$ [57]. The non-homogeneity functions in the layers are given as: $\eta^{(k+1)}(z_1)=z_1^2$.

The magnitudes of dimensionless BFEFs of LNHOCSs are compared with those of LHOCSs with by estimating the percentage differences of the magnitudes of excitation frequencies, respectively, as $100\%\times(\overline{\Lambda}_{1jNH}-\overline{\Lambda}_{1jH})/\overline{\Lambda}_{1jH}$.

The distributions of dimensionless BFEFs, $\overline{\Lambda}_{ij}(i=1,j=1,2)$, for LNHOCSs with the parabolic material profile made of one, three and four plies of Glass-Epoxy oriented according to the following

Table 2
Comparison of the DFP, ω_1, for anti-symmetric cross-ply LHOCSs.

$\omega_1 = \omega R_2\sqrt{[1-\nu_{r\theta}^{(k+1)}\nu_{\theta r}^{(k+1)}]\rho_0^{(k+1)}/E_{0r}^{(k+1)}}$					
$(0/9)_2$			$(0/9)_{10}$		
Shu [5]	Wu and Lee [29] DQM (N = 7)	Present Study	Shu [5]	Wu and Lee [29] DQM (N = 7)	Present Study
0.1799	0.1875	0.1750	0.1976	0.2019	0.2043

Table 3
Comparison of the DFP for LHO cylindrical shells with lamination schemes (0/9/0) and (0/9/9/0).

R/L_1	5	10	5	10
Stacking sequence	(0/9/0)	(0/9/0)	(0/9/9/0)	(0/9/9/0)
Ferreira et al. [14]	20.4856	16.8531	20.5202	16.8441
Ye and Soldatos [60]	–	–	19.977 (18)	16.486 (28)
Present study	19.588 (20)	16.6709 (31)	20.0758 (18)	16.5563 (28)

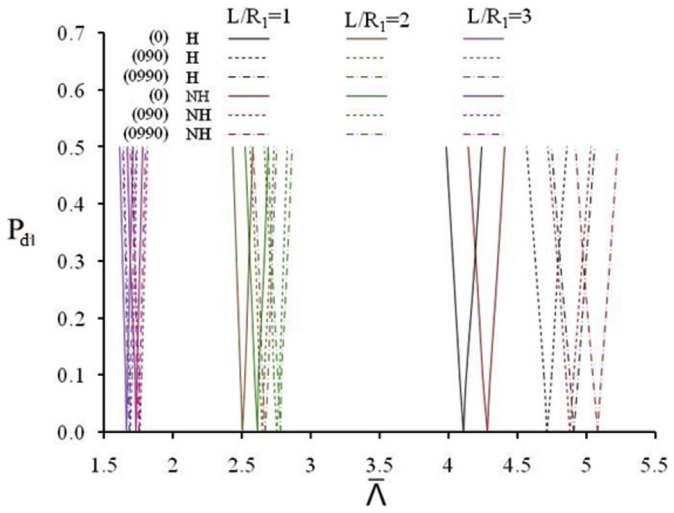

Fig. 2. Distributions of BFFEs of LNHOCSs depending on the L/R_1.

schemes (0), (0/9/0) and (0/9/9/0), depending on the P_{d1} are presented in the current analysis and illustrated in Fig. 2. The LNHOCS characteristics are, $L = R_1, 2R_1, 3R_1$, $R_1 = 100h$ and $\gamma = 15^\circ$. The static axial load factor $P_{s1} = 0.2$ and the wave numbers $(m,n) = (1,2)$ are considered. It is important to underline the fact that the values of dimensionless BFEFs of LNHOCSs decrease monotonically, as the L increases from R_1 to $3R_1$. The influences of non-homogeneity on the values of dimensionless BFEFs irregularly vary, while the area of the main instability regions decrease with the increasing of the ratio, L/R_1. The greatest effect of non-homogeneity on the values of $\overline{\Lambda}_{ij}(i = 1, j = 1,2)$ takes 4.4% occurs in the single orthotropic layer arranged as (0) takes 4.14% occurs in the lamination scheme (0/9/0) and is 4.26% occurs in four plies arranged as (0/9/9/0), whereas, the lowest effects are 3.68%, 3.28% and 3.36% occur in the lamination schemes (0), (0/9/0) and (0/9/9/0), respectively, as the L varies between R_1 and $3R_1$. The influences of laminations schemes (0/9/0) and (0/9/9/0) on the dimensionless values of BFEFs compared to the (0) single-layer orthotropic conical shell are significant and are reduced from about 15% to 1.8% and from about 19.6% to 1.2% for the homogeneous case, while their effects are reduced from about 14% to 1.7% and from about 1.16% to 18.8%, respectively, for the NH case, as the L increases from R_1 to $3R_1$.

The distributions of dimensionless BFEFs of LNHOCSs with laminations (0), (0/9/0) and (0/9/9/0), against the P_{d1} for different P_{s1} are calculated and depicted in Fig. 3. The data are $R_1/h = 100$, $L/R_1 = 2$, $\gamma = 30^\circ$ and wave numbers $(m,n) = (1,3)$ are considered. The magnitudes of dimensionless BFEFs of LNHOCSs and LHOCSs decrease, as the static axial load factor, P_{s1}, increases. As the P_{d1} increment from 0 to 0.6, the dimensionless backward frequency, $\overline{\Lambda}_{11}$, for LNHOCSs and LHOCSs decreases, whereas, the magnitudes of the dimensionless forward excitation frequency, $\overline{\Lambda}_{12}$, increases. As the magnitudes of $\overline{\Lambda}_{ij}(i = 1, j = 1,2)$ for LNHOCSs are compared with those of LHOCSs, the influences of non-homogeneity on the dimensionless BFEFs vary irregularly, as the axial load factors P_{d1} and P_{s1} increase. The highest influences of non-homogeneity on the magnitudes of dimensionless BFEFs for LNHOCSs with laminations (0) and (0/9/0) are (4.8%) and (4.9%) for $P_{d1} = 0.4$ and $P_{s1} = 0.5$, respectively, and for the lamination (0/9/9/0) highest influence is (4.6%) for $P_{d1} = 0.4$ and $P_{s1} = 0.1$. It should be pointed out that the field of main instability regions decrease with the increasing of the static axial factor.

The distributions of dimensionless BFEFs of LNHOCSs and LHOCSs with the plies arranged as (0), (0/9/0) and (0/9/9/0), depending on the ratio, R_1/h, are shown in Fig. 4. The conical shell and load parameters are $L/R_1 = 2$, $\gamma = 30^\circ$, $P_{s1} = 0.2$ and $(m,n) = (1,2)$. The values of dimensionless BFEFs of LNHOCSs and LHOCSs conical shells diminish, as R_1/h increment. When the LNHOCSs with laminations (0), (0/9/0) and (0/9/9/0) are compared with those of LHOCSs, the greatest effect of non-homogeneity on the values of dimensionless backward or forward excitation frequencies is about 4.1% occurs in the single orthotropic layer arranged as (0), is about 3.5% occurs in three plies arranged as (0/9/0) and is about 3.6% occurs in four plies arranged as (0/9/9/0), respectively, when the ratio, R_1/h, varies between 50 and 150. The influences of laminations schemes (0/9/0) and (0/9/9/0) on the

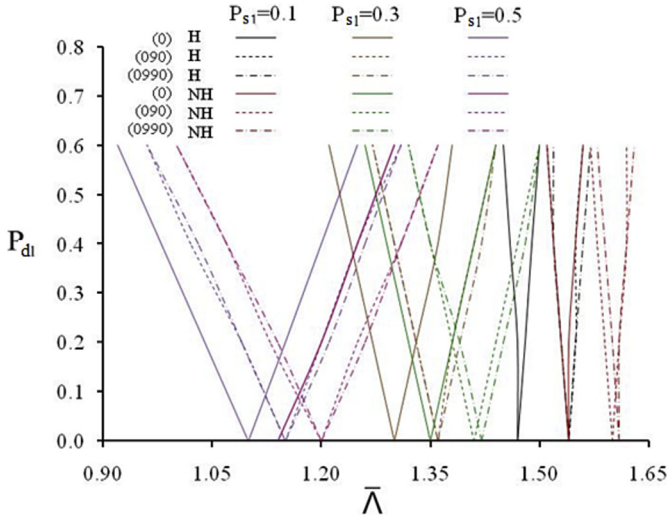

Fig. 3. Distributions of dimensionless BFFEs of LNHOCSs with different lamination schemes against the P_{d1}.

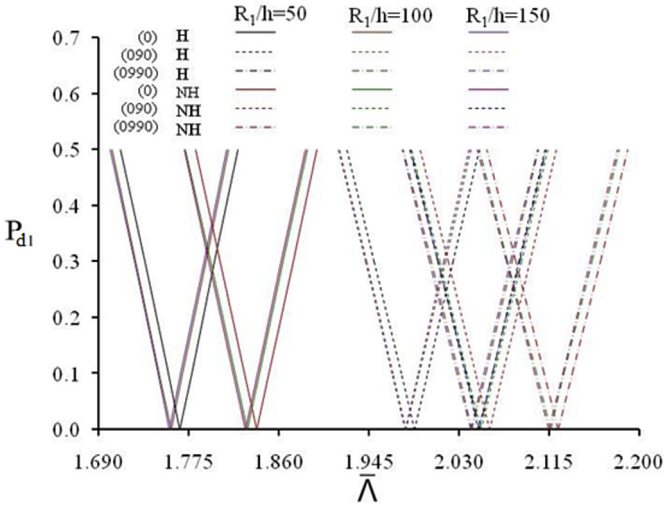

Fig. 4. Distributions of BFFEs of LNHOCSs depending on the R_1/h.

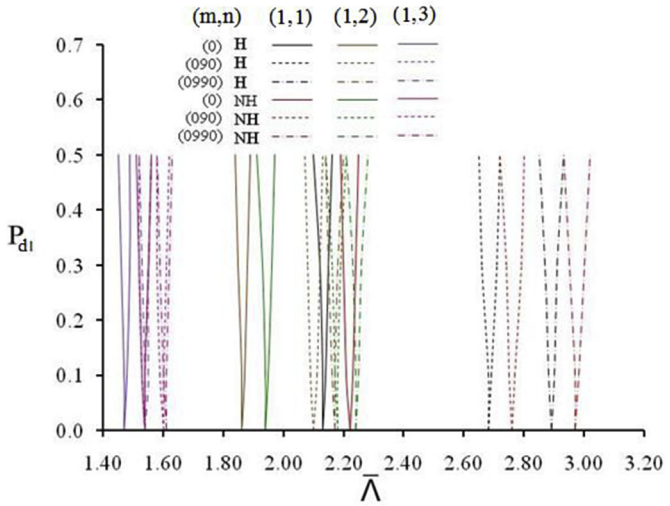

Fig. 6. Distributions of dimensionless BFFEs of LNHOCSs depending on the circumferential wave number, n.

dimensionless values of BFEFs compared to the (0) single-layer orthotropic conical shell remain constant and are about 12.6% and 16% for the homogeneous case, while their effects are about 12% and 15.6% for the non-homogeneous case, respectively, as the ratio of R_1/h increases from 50 to 150.

In this example, examined the influences of the material non-homogeneity and material orientation on the magnitudes of dimensionless BFEFs of LNHOCS and LHOCS for different the semi-vertex angle, γ, and are plotted in Fig. 5. The following conical shell and load parameters are used in the calculations: $R_1 = 100h$, $L = 2R_1$, $h = 0.01m$, $\gamma = 15^\circ, 30^\circ, 45^\circ$, $P_{s1} = 0.1$, P_{d1} changes from 0.1 to 0.5 with the step 0.2 and (m, n)=(1,2). Two different stacking sequences are considered: (0/9/0) and (0/9/9/0). In addition, the case of single orthotropic ply oriented of (0) is also considered to emphasize the influence of the lamination scheme on the magnitudes of dimensionless BFEFs of orthotropic cylindrical and conical shells. It can be seen that the magnitudes of dimensionless BFEFs of conical shells decrease with the increasing of the semi-vertex angle, γ from 15° to 45°. It is evident that the sizes of main instability regions decrease, whereas, the influences of non-homogeneity on the magnitudes of dimensionless BFEFs of conical shells irregularly change, as the semi-vertex angle, γ, changes between 15° and 45°. The greatest influence of heterogeneity on the values of BFEFs is 4.9% occurs in the single orthotropic layer (0), highest effect is 4.26% occurs in the stacking sequence (0/9/0) and highest effect is 4.26% occurs in the stacking sequence (0/9/9/0), whereas, the lowest effects are 3.8%, 2.3% and 2.7% occur in the stacking sequences (0), (0/9/0) and (0/9/9/0), respectively, as the semi-vertex angle, γ, changes between 15° and 45°. As the BFEFs of laminated conical shells with the schemes (0/9/0) and (0/9/9/0) compared to those of the single orthotropic conical shell with the orientation (0), the effects of the stacking sequences on the values of frequencies increase from about 5.7% to 24.7% and from about 6.4% to 33.6% for the homogeneous case, while those increase from about 5.4% to 23.8% and from about 6.5% to 32%, respectively, for the non-homogeneous case, as the γ increases from 15° and 45°.

The effects of the variation of the wave numbers, (m, n), on the dimensionless BFEFs of LNHOCSs and LHOCSs for the stacking sequences (0), (0/9/0) and (0/9/9/0), are shown in Figs. 6 and 7. The conical shell characteristics are, $\gamma = 30^\circ$, $R_1h = 100h$ and $L = 2R_1$. The axial static load factor is taken to be $P_{s1} = 0.1$. It is possible to observe that the values of BFEFs of LNHOCSs and LHOCSs for the stacking sequences (0/9/0) and (0/9/9/0), decrease with the

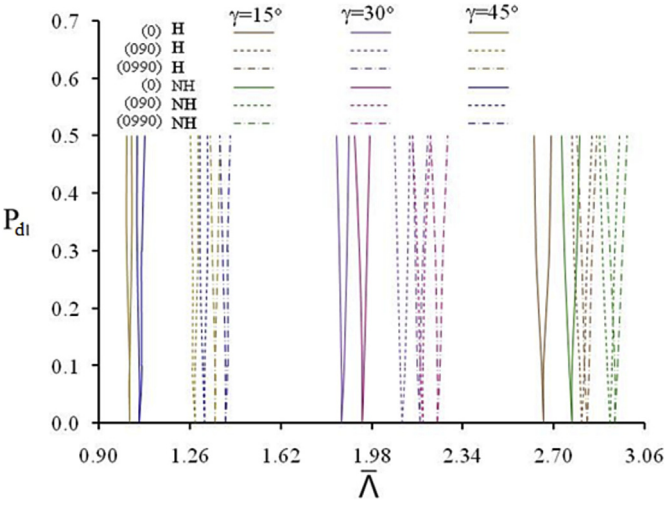

Fig. 5. Distributions of dimensionless BFFEs of LNHOCSs depending on the γ.

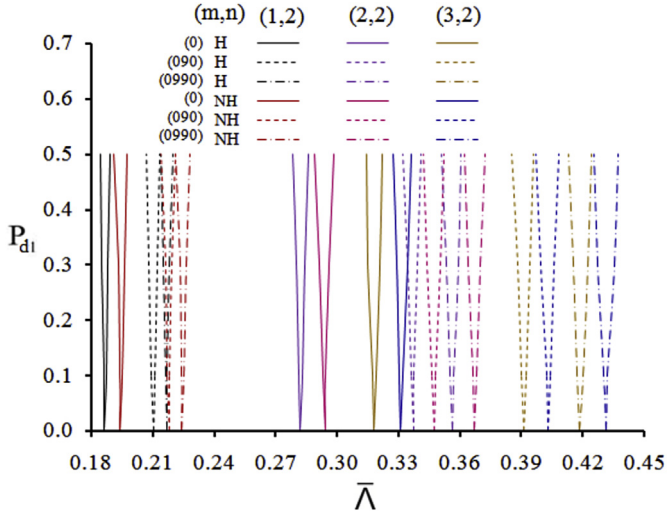

Fig. 7. Distributions of dimensionless BFFEs of LNHOCSs depending on the meridional wave number, m.

increasing of n from 1 to 3 for fixed values of m ($m = 1$), whereas these values significantly increase with the increasing of m from 1 to 3 for fixed values of n ($n = 2$). The influences of non-homogeneity on the magnitudes of dimensionless BFEFs of LNHOCSs for the stacking sequences (0/9/0) and (0/9/9/0) increase regularly, as n increases from 1 to 3, whereas, these influences vary irregularly, as m increases from 1 to 3. For example, as the circumferential wave number, n, increases from 1 to 3, the influences of non-homogeneity on the values of $\overline{\Lambda}_{11}$ (and $\overline{\Lambda}_{12}$) increase from 2.61% (and 2.97%) to 3% and from 3.1% (and 2.76%) to 3.9% for $P_{d1} = 0.1$, at the stacking sequences (0/9/0) and (0/9/9/0), respectively. As the meridional wave number, m, increases from 1 to 3, the influences of non-homogeneity on the values of $\overline{\Lambda}_{11}$ (and $\overline{\Lambda}_{12}$) diminish from 3.83% (and 3.32%) to 3.07% and from 3.7% to 3.12 (and 2.86%) at the stacking sequences (0/9/0) and (0/9/9/0), respectively, for $P_{d1} = 0.1$. As the BFEFs of the single-layer (0) orthotropic conical shell are compared with those of lamination schemes (0/9/0) and (0/9/9/0), the effects of the stacking sequences on the values of $\overline{\Lambda}_{ij}(i = 1, j = 1, 2)$ are reduced from about 25.47% to 4% and from about 35.4% to 4.8% for the homogeneous profile, while those decrease from about 24.5% to 3.9% and from about 34% to 4.55%, respectively, for the non-homogeneous profile, as the n increases 1 to 3 (see, Fig. 6), while these effects increment from about 12% to 23% and from about 16% to 32% for the homogeneous profile, while those increase from about 12% to 21.4% and from about 15.5% to 30.3%, respectively, for the non-homogeneous profile, as the m increases 1 to 3 (see, Fig. 7), for $P_{d1} = 0.3$.

6. Conclusion

The excitation frequencies of parametric vibration of LNHOCSs under axial load periodically varying with time are determined using the CST. The basic equations are derived using the Donnell-Mushtari shell theory and reduce to the Mathieu-Hill type differential equation, in which the instability is examined by the Bolotin method. To validate of current results was made a comparison with the previous studies. The effects of stacking sequences, axial load factors, non-homogeneity, as well as the variation of geometric characteristics on the BFEFs of LNHOCSs are studied in detail.

Appendix A

In Eq. (10), $L_{ij}(i,j = 1,2,\ldots,4)$ are expressed as

$$
\begin{aligned}
L_{11} &= \xi_{12}e^{2x}\frac{\partial^4}{\partial x^4} + (\xi_{11} + 4\xi_{12} - \xi_{22})e^{2x}\frac{\partial^3}{\partial x^3} + (3\xi_{11} + 5\xi_{12} - 3\xi_{22} - \xi_{21})e^{2x}\frac{\partial^2}{\partial x^2} \\
&+2(\xi_{11} + \xi_{12} - \xi_{22} - \xi_{21})e^{2x}\frac{\partial}{\partial x} + \left(\frac{\partial^2}{\partial x^2} + 3\frac{\partial}{\partial x} + 2\right)r_1 e^{3x}\cot\gamma + \xi_{21}e^{2x}\frac{\partial^4}{\partial\theta_1^4} \\
&+(\xi_{11} - 2\xi_{31} + \xi_{22})e^{2x}\frac{\partial^4}{\partial x^2\partial\theta_1^2} + (\xi_{11} - 4\xi_{31} + 3\xi_{22})e^{2x}\frac{\partial^3}{\partial x\partial\theta_1^2} \\
&+2(\xi_{22} - \xi_{31} + \xi_{21})e^{2x}\frac{\partial^2}{\partial\theta_1^2}, \\
L_{12} &= -\xi_{24}\frac{\partial^4}{\partial\theta_1^4} - (\xi_{14} + \xi_{23} + 2\xi_{32})\frac{\partial^4}{\partial x^2\partial\theta_1^2} + (3\xi_{14} + \xi_{23} + 4\xi_{32})\frac{\partial^3}{\partial x\partial\theta_1^2} \\
&-2(\xi_{14} + \xi_{32} + \xi_{24})\frac{\partial^2}{\partial\theta_1^2} - \xi_{13}\frac{\partial^4}{\partial x^4} + 4(\xi_{13} + \xi_{23} - \xi_{14})\frac{\partial^3}{\partial x^3} \\
&-(5\xi_{13} + 3\xi_{23} - 3\xi_{14} - \xi_{24})\frac{\partial^2}{\partial x^2} + 2(\xi_{13} + \xi_{23} - \xi_{14} - \xi_{24})\frac{\partial}{\partial x} \\
&-e^{2x}r_1^2[P_s + P_d\cos(\Lambda t)]\left(\frac{\partial^2}{\partial x^2} - \frac{\partial}{\partial x}\right) - r_1^4 e^{4x}\rho_1\frac{\partial^2}{\partial t^2} = 0, \qquad \text{(A1)} \\
L_{21} &= \vartheta_{22}e^{2x}\frac{\partial^4}{\partial x^4} - 4\vartheta_{22}e^{2x}\frac{\partial^3}{\partial x^3} + (5\vartheta_{22} - \vartheta_{11})e^{2x}\frac{\partial^2}{\partial x^2} + 2(\vartheta_{11} - \vartheta_{22})e^{2x}\frac{\partial}{\partial x} \\
&+2(\vartheta_{31} + \vartheta_{12})e^{2x}\frac{\partial^4}{\partial x^2\partial\theta_1^2} - 4(\vartheta_{31} + \vartheta_{12})e^{2x}\frac{\partial^3}{\partial x\partial\theta_1^2} \\
&+2(\vartheta_{31} + \vartheta_{12} + \vartheta_{11})e^{2x}\frac{\partial^2}{\partial\theta_1^2} + \vartheta_{11}e^{2x}\frac{\partial^4}{\partial\theta_1^4} \\
L_{22} &= -\vartheta_{14}\frac{\partial^4}{\partial\theta_1^4} + (2\vartheta_{32} - \vartheta_{13} - \vartheta_{24})\frac{\partial^4}{\partial x^2\partial\theta_1^2} + (3\vartheta_{24} - 4\vartheta_{32} + \vartheta_{13})\frac{\partial^3}{\partial x\partial\theta_1^2} \\
&+2(\vartheta_{32} - \vartheta_{24} - \vartheta_{14})\frac{\partial^2}{\partial\theta_1^2} - \vartheta_{23}\frac{\partial^4}{\partial x^4} + (\vartheta_{13} - \vartheta_{24} + 4\vartheta_{23})\frac{\partial^3}{\partial x^3} + \\
&+(3\vartheta_{24} - 3\vartheta_{13} - 5\vartheta_{23} + \vartheta_{14})\frac{\partial^2}{\partial x^2} + 2(\vartheta_{13} + \vartheta_{23} - \vartheta_{14} - \vartheta_{24})\frac{\partial}{\partial x} \\
&+r_1 e^x\cot\gamma\left(\frac{\partial^2}{\partial x^2} - \frac{\partial}{\partial x}\right) = 0
\end{aligned}
$$

where the following quantities entered here:

$$\begin{aligned}
&\xi_{11}=A_{111}\vartheta_{11}+A_{121}\vartheta_{21},\xi_{12}=A_{111}\vartheta_{12}+A_{121}\vartheta_{22},\xi_{13}=A_{111}\vartheta_{13}+A_{121}\vartheta_{23}+A_{112},\\
&\xi_{14}=A_{111}\vartheta_{14}+A_{121}\vartheta_{24}+A_{122},\xi_{21}=A_{211}\vartheta_{11}+A_{221}\vartheta_{21},\xi_{22}=A_{211}\vartheta_{12}+A_{221}\vartheta_{22},\\
&\xi_{23}=A_{211}\vartheta_{13}+A_{221}\vartheta_{14}+A_{212},\xi_{24}=A_{211}\vartheta_{14}+A_{221}\vartheta_{13}+A_{222},\xi_{31}=A_{661}\vartheta_{31},\\
&\xi_{32}=A_{661}\vartheta_{32}+A_{662},\vartheta_{11}=A_{220}/L_0,\vartheta_{12}=-A_{12}^0\Big/L_0,\vartheta_{13}=(A_{120}A_{121}-A_{111}A_{220})/L_0,\\
&\vartheta_{14}=(A_{120}A_{221}-A_{121}A_{220})/L_0,\vartheta_{21}=-A_{210}/L_0,\vartheta_{22}=A_{110}/L_0,\\
&\vartheta_{23}=(A_{210}A_{111}-A_{211}A_{110})/L_0,\vartheta_{24}=(A_{210}A_{121}-A_{221}A_{210})/L_0,\\
&\vartheta_{31}=1/A_{660},\vartheta_{32}=-A_{661}/A_{660},L_0=A_{110}A_{220}-A_{120}A_{210}
\end{aligned} \tag{A2}$$

in which expressions $A_{ijk_1}(k_1=0,\ 1,\ 2;\ i,j=1,2,6)$ are defined as follows:

$$\begin{aligned}
&A_{11k_1}=h^{k_1+1}\sum_{k=0}^{N-1}\frac{E_{0r}^{(k+1)}\hbar^{(k+1)}}{1-\nu_{r\theta}^{(k+1)}\nu_{\theta r}^{(k+1)}},\quad A_{12k_1}=h^{k_1+1}\sum_{k=0}^{N-1}\frac{\nu_{\theta r}^{(k+1)}E_{0r}^{(k+1)}\hbar^{(k+1)}}{1-\nu_{r\theta}^{(k+1)}\nu_{\theta r}^{(k+1)}},\\
&A_{21k_1}=h^{k_1+1}\sum_{k=0}^{N-1}\frac{\nu_{r\theta}^{(k+1)}E_{0\theta}^{(k+1)}\hbar^{(k+1)}}{1-\nu_{r\theta}^{(k+1)}\nu_{\theta r}^{(k+1)}},\quad A_{22k_1}=h^{k_1+1}\sum_{k=0}^{N-1}\frac{E_{0\theta}^{(k)}\hbar^{(k+1)}}{1-\nu_{r\theta}^{(k+1)}\nu_{\theta r}^{(k+1)}},\\
&A_{66k_1}=h^{k_1+1}\sum_{k=0}^{N-1}G_0^{(k+1)}\hbar^{(k+1)},\hbar^{(k+1)}=\int_{-1/2+k/N}^{1/2+(k+1)/N}z_1^{k_1}\eta_1^{(k+1)}dz_1
\end{aligned} \tag{A3}$$

Appendix B

In Eq. (16), K, u_{ax} and u_ρ are parameters and expressed as

$$\begin{aligned}
&K=(3K_3-2m_1K_1)\frac{u_1}{3}+(K_2-m_1K_4)u_2+u_3,\\
&u_{ax}=r_1^2\left(1+\frac{m_1^2}{2}\right)\frac{m_1^2}{4\left(m_1^2+4\right)}\left(e^{4x_0}-1\right),u_\rho=\frac{r_1^4m_1^2}{12\left(m_1^2+9\right)}\left(e^{6x_0}-1\right)
\end{aligned} \tag{B1}$$

in which

$$
\begin{aligned}
K_1 &= U_1\xi_{12}m_1^4 + U_2m_1^3(\xi_{11}-\xi_{22}+4\xi_{12})\\
&-U_1m_1^2(4\xi_{12}+3\xi_{11}-3\xi_{22})-\\
&\quad -2U_2m_1(\xi_{11}-\xi_{22}) + U_1m_2^4\xi_{21}\\
&+U_1m_1^2m_2^2(\xi_{11}-2\xi_{31}+\xi_{22})+\\
&\quad +U_2m_1m_2^2(\xi_{11}-4\xi_{31}+3\xi_{22}) - 2U_1m_2^2(\xi_{22}-\xi_{31}+\xi_{12})\\
&\quad -\left(U_3m_1^2+U_4m_1\right)r_1\cot\gamma,\\
K_2 &= U_3\left(m_1^4+2m_1^2+1+m_2^4-2m_2^2\right)\xi_{12}\\
&+U_4\left(m_1^3+m_1-m_1m_2^2\right)(\xi_{11}-\xi_{22})\\
&\quad +U_3m_1^2m_2^2(\xi_{11}-2\xi_{31}+\xi_{22}) - \xi_{13}m_1^4-\\
&(\xi_{13}+\xi_{24})m_1^2 - \xi_{24}m_2^4\\
&\quad -m_1^2m_2^2(\xi_{14}+\xi_{23}+2\xi_{32}) + 2\xi_{24}m_2^2,\\
K_3 &= U_2\xi_{12}m_1^4 - U_1m_1^3(\xi_{11}-\xi_{22}+4\xi_{12})\\
&-U_2m_1^2(5\xi_{12}+3\xi_{11}-3\xi_{22}-\xi_{21})+\\
&\quad +2U_1m_1(\xi_{11}-\xi_{22}+\xi_{12}-\xi_{21})\\
&+U_2\beta_1^2m_2^2(\xi_{11}-2\xi_{31}+\xi_{22}) + U_2m_2^4\xi_{21}-\\
&\quad -U_1m_1m_2^2(3\xi_{22}-4\xi_{31}+\xi_{11}) - 2U_2m_2^2(\xi_{22}-\xi_{31}+\xi_{21})\\
&\quad +\left(U_3m_1-U_4m_1^2\right)r_1\cot\gamma,\\
K_4 &= U_4\left(m_1^4+2m_1^2+1+m_2^4-2m_2^2\right)\xi_{12}\\
&+U_3\left(m_1m_2^2-m_1^3-m_1\right)(\xi_{11}-\xi_{22})\\
&\quad +U_4m_1^2m_2^2(\xi_{11}-2\xi_{31}+\xi_{22})\\
&+(\xi_{14}-\xi_{23})\left[m_1+m_1^3-m_1m_2^2\right],
\end{aligned}
$$

$$
u_1 = \frac{m_1}{4m_1^2+9}\left(e^{3x_0}-1\right), u_2 = \frac{m_1^2}{4(m_1^2+1)}\left(1-e^{2x_0}\right),
$$

$$
\begin{aligned}
u_3 &= -\left[\left(2U_1-3U_2m_1-U_1m_1^2\right)\frac{m_1}{2}+\left(U_2m_1^2-3U_1m_1-2U_2\right)\right]\\
&\quad\times\frac{m_1}{4(m_1^2+4)}\left(e^{4x_0}-1\right)r_1\cot\gamma
\end{aligned}
\tag{B2}
$$

References

[1] Hui D, Du IHY. Effects of axial imperfections on vibrations of anti-symmetrical cross-ply, oval cylindrical-shells. J Appl Mech 1986;53:675–80.
[2] Hui D. Effects of shear loads on vibration and buckling of antisymmetric cross-ply cylindrical panels. Int J Non Lin Mech 1988;23:177–87.
[3] Kayran A, Vinson JR. Free vibration analysis of laminated composite truncated circular conical shells. AIAA J 1990;28:1259–69.
[4] Tong L. Free vibration of composite laminated conical shells. Int J Mech Sci 1993;35:47–61.
[5] Shu C. Free vibration analysis of composite laminated conical shells by generalized differential quadrature. J Sound Vib 1996;194:587–604.
[6] Wu CP, Wu CH. Asymptotic differential quadrature solutions for the free vibration of laminated conical shells. Comput Mech 2000;25:346–57.
[7] Hua L, Lam KY. Orthotropic influence on frequency characteristics of a rotating composite laminated conical shell by the generalized differential quadrature method. Int J Solid Struct 2001;38:3995–4015.
[8] Hu HT, Ou SC. Maximizations of fundamental frequency of laminated truncated conical shells with respect to fiber orientation. Compos Struct 2001;52:265–75.
[9] Correia IFP, Mota Soares CM, Mota Soares CA, Hreskovits J. Analysis of laminated conical shell structures using higher order models. Compos Struct 2003;62:383–90.
[10] Ng TY, Li H, Lam KY. Generalized differential quadrature for free vibration of rotating composite laminated conical shell with various boundary conditions. Int J Mech Sci 2003;45:567–87.
[11] Civalek Ö. Free vibration analysis of composite conical shells using the discrete singular convolution algorithm. Steel Compos Struct 2006;6:353–66.
[12] Sofiyev AH, Kuruoglu N. Natural frequency of laminated orthotropic shells with different boundary conditions and resting on the Pasternak type elastic foundation. Compos B Eng 2011;42:1562–70.
[13] Ferreira AJM, Carrera E, Cinefra M, Roque CMC, Polit O. Analysis of laminated shells by a sinusoidal shear deformation theory and radial basis functions collocation, accounting for through-the- thickness deformations. Compos Part B-Eng 2011;42:1276–84.
[14] Shariyat M. An accurate double-superposition global-local theory for vibration and bending analyses of cylindrical composite and sandwich shells subjected to thermo-mechanical loads. Proc IME C J Mech Eng Sci 2011;225(C8):1816–32.
[15] Viswanathan KK, Lee JH, Aziz ZA, Hossain I, Wang R, Abdullah HY. Vibration analysis of cross-ply laminated truncated conical shells using a spline method. J Eng Math 2012;76:139–56.
[16] Civalek Ö. Vibration analysis of laminated composite conical shells by the method of discrete singular convolution based on the shear deformation theory. Compos B Eng 2013;45:1001–9.
[17] Zarouni E, Jalilian Rad M, Tohidi H. Free vibration analysis of fiber reinforced composite conical shells resting on Pasternak-type elastic foundation using Ritz and Galerkin methods. Int J Mech Mater Des 2014;10:421–38.
[18] Fazzolari FA. A refined dynamic stiffness element for free vibration analysis of cross-ply laminated composite cylindrical and spherical shallow shells. Compos B Eng 2014;62:143–58.
[19] Viswanathan KK, Sair J, Izliana AB, Zainal AA. Free vibration of anti-symmetric angle-ply laminated conical shells. Compos Struct 2015;122:488–95.
[20] Wu S, Qu Y, Hua H. Free vibration of laminated orthotropic conical shell on Pasternak foundation by a domain decomposition method. J Compos Mater 2015;49:35–52.
[21] Tornabene F. General higher order layer-wise theory for free vibrations of doubly-curved laminated composite shells and panels. Mech Adv Mater Struct 2016;23:1046–67.
[22] Tornabene F, Fantuzzi N, Bacciocchi M. On the mechanics of laminated doubly-curved shells subjected to point and line loads. Int J Eng Sci 2016;109:115–64.
[23] Tornabene F, Fantuzzi N, Bacciocchi M, Neves AMA, Ferreira AJM. MLSDQ Based on RBFs for the free vibrations of laminated composite doubly-curved shells. Compos B Eng 2016;99:30–47.
[24] Tornabene F, Fantuzzi N, Bacciocchi M, Viola E. Effect of agglomeration on the natural frequencies of functionally graded carbon nanotube-reinforced laminated composite doubly-curved shells. Compos B Eng 2016;89:187–218.
[25] Samsonov AM, Semenova IV, Garbuzov FE. Nonlinear guided bulk waves in heterogeneous elastic structural elements. Int J Non-Lin Mech 2017 (in press), https://doi.org/10.1016/j.ijnonlinmec.2017.01.012.
[26] Lomakin VA. The elasticity theory of non-homogeneous materials. Moscow: Nauka; 1976 (in Russian).
[27] Khoroshun LP, Kozlov SY, Ivanov YA, Koshevoi IK. The generalized theory of plates and shells non-homogeneous in thickness direction. Kiev: Naukova Dumka; 1988 (in Russian).
[28] Baruch M, Arbocz J, Zhang GQ. Laminated conical shells – considerations for the variations of stiffness coefficients. Report LR-671. The Netherlands: Faculty of Aerospace Engineering, Delft University of Technology; 1992.
[29] Wu CP, Lee CY. Differential quadrature solution for the free vibration analysis of laminated conical shells with variable stiffness. Int J Mech Sci 2001;43:1853–69.
[30] Sofiyev AH, Schnack E. The buckling of cross-ply laminated non-homogeneous orthotropic composite conical thin shells under a dynamic external pressure. Acta Mech 2003;162:29–40.
[31] Tripathi V, Singh BN, Shukla KK. Free vibration of laminated composite conical shells with random material properties. Compos Struct 2007;81:96–104.
[32] Sofiyev AH, Karaca Z. The vibration and stability of laminated non-homogeneous orthotropic conical shells subjected to external pressure. Eur J Mech Solids 2009;28:317–28.
[33] Akhavan H, Ribeiro P. Natural modes of vibration of variable stiffness composite laminates with curvilinear fibers. Compos Struct 2011;93:3040–7.
[34] Sofiyev AH, Kuruoglu N. Combined influences of shear deformation, rotary inertia and heterogeneity on the frequencies of cross-ply laminated orthotropic cylindrical shells. Compos B Eng 2014;66:500–10.
[35] Bakulin VN, Ostrik AV. The combined thermal and mechanical effect of radiation and shockwaves on a multilayer orthotropic shell with a heterogeneous coating. J Appl Math Mech 2014;78:155–62.
[36] Fazzolari FA. Reissner's mixed variational theorem and variable kinematics in the modelling of laminated composite and FGM doubly-curved shells. Compos B Eng 2016;89:408–23.
[37] Marouene A, Boukhili R, Chen J, Yousefpour A. Effects of gaps and overlaps on the buckling behavior of an optimally designed variable-stiffness composite laminates – a numerical and experimental study. Compos Struct 2016;140:556–66.
[38] Vescovini R, Dozio L. A variable-kinematic model for variable stiffness plates:

vibration and buckling analysis. Compos Struct 2016;142:15–26.
[39] Carrera E, Pagani A, Valvano S. Shell elements with through-the-thickness variable kinematics for the analysis of laminated composite and sandwich structures. Compos B Eng 2017;111:294–314.
[40] Goroshko OA, Emelyanenko VV. Dynamic stability of layered anisotropic shells. Sov Appl Mech 1975;3:720–5.
[41] Argento A, Scott RA. Dynamic instability of layered anisotropic circular cylindrical shells. Part I: theoretical development. J Sound Vib 1993;162:311–22.
[42] Argento A, Scott RA. Dynamic instability of layered anisotropic circular cylindrical shells. Part II: numerical results. J Sound Vib 1993;162:323–32.
[43] Liao CL, Cheng CR. Dynamic stability of stiffened laminated composite plates and shells subjected to in-plane pulsating forces. J Sound Vib 1994;174:335–51.
[44] Liao CL, Cheng CR. Dynamic stability of stiffened laminated composite plates and shells subjected to in-plane pulsating forces. Int J Numer Meth Eng 1994;37:4167–83.
[45] Lam KY, Ng TY. Dynamic stability analysis of laminated composite cylindrical shells subjected to conservative periodic axial loads. Compos B Eng 1998;29B:769–85.
[46] Ng TY, Lam KY. Dynamic stability analysis of cross-ply laminated cylindrical shells using different thin shell theories. Acta Mech 1999;134:147–67.
[47] Sahu SK, Datta PK. Research advances in the dynamic stability behavior of plates and shells: 1987–2005-Part I: conservative systems. Appl Mech Rev 2007;60:65–75.
[48] Fazilati J, Ovesy HR. Dynamic instability analysis of composite laminated thin walled structures using two versions of FSM. Compos Struct 2010;92:2060–5.
[49] Ovesy HR, Fazilati J. Parametric instability analysis of laminated composite curved shells subjected to non-uniform in-plane load. Compos Struct 2014;108:449–55.
[50] Dey T, Ramachandra LS. Static and dynamic instability analysis of composite cylindrical shell panels subjected to partial edge loading. Int J Non Lin Mech 2014;64:46–56.
[51] Panda HS, Sahu SK, Parhi PK. Hygrothermal response on parametric instability of delaminated bidirectional composite flat panels. Eur J Mech Solid 2015;53:268–81.
[52] Park WT, Han SC, Jung WY, Lee WH. Dynamic instability analysis for S-FGM plates embedded in Pasternak elastic medium using the modified couple stress theory. Steel Compos Struct 2016;22(6):1239–59.
[53] Lei ZX, Zhang LW, Liew KM. Parametric analysis of frequency of rotating laminated CNT reinforced functionally graded cylindrical panels. Compos B Eng 2016;90:251–66.
[54] Sahmani S, Aghdam MM. Nonlinear instability of hydrostatic pressurized hybrid FGM exponential shear deformable nanoshells based on nonlocal continuum elasticity. Compos B Eng 2017;114:404–17.
[55] Li C, Liu JJ, Cheng M, Fan XL. Nonlocal vibrations and stabilities in parametric resonance of axially moving viscoelastic piezoelectric nanoplate subjected to thermo-electro-mechanical forces. Compos B Eng 2017;116:153–69.
[56] Akhavan H, Ribeiro P. Geometrically non-linear periodic forced vibrations of imperfect laminates with curved fibres by the shooting method. Compos B Eng 2016;109:286–96.
[57] Reddy JN. Mechanics of laminated composite plates and shells: theory and analysis. second ed. CRC Press; 2004.
[58] Agamirov VL. Dynamic problems of non-linear shells theory. Moscow: Nauka; 1990 (in Russian).
[59] Bolotin VV. The dynamic stability of elastic systems. San Francisco, CA: Holden-Day; 1964.
[60] Ye JQ, Soldatos KP. Three-dimensional vibrations of laminated cylinders and cylindrical panels with a symmetric or an anti-symmetric cross-ply lay-up. Compos Eng 1994;4:429–44.